Journal of the Korean Ceramic Society
Vol. 52, No. 5, pp. 320~324, 2015.

http://dx.doi.org/10.4191/kcers.2015.52.5.320

Fabrication of NiO-Y:$BaZrO_3$ Composite Anode for Thin Film-Protonic Ceramic Fuel Cells using Tape-Casting

Kiho Bae*,, Ho-Sung Noh**, Dong Young Jang*, Manjin Kim*, Hyun Joong Kim*, Jongsup Hong**, Jong-Ho Lee**, Byung-Kook Kim**, Ji-Won Son**,†, and Joon Hyung Shim*,‡**

**School of Mechanical Engineering, Korea University, Seoul 02841, Korea*

***High-temperature Energy Materials Research Center, Korea Institute of Science and Technology (KIST), Seoul 02792, Korea*

(Received July 23, 2015; Revised August 6, 2015; Accepted August 7, 2015)

ABSTRACT

Optimization of the fabrication process of NiO-yttrium doped barium zirconate (BZY) composite anode substrates using tape-casting for high performance thin-film protonic ceramic fuel cells (PCFCs) is investigated. The anode substrate is composed of a tens of microns-thick anode functional layer laminated over a porous anode substrate. The macro-pore structure of the anode support is induced by micron-scale polymethyl methacrylate (PMMA) pore formers. Thermal gravity analysis (TGA) and a dilatometer are used to determine the polymeric additive burn-out and sintering temperatures. Crystallinity and microstructure of the tape-cast NiO-BZY anode are analyzed after the sintering.

Key words : NiO-BZY, Protonic ceramic fuel cells, Composite anode supports, Tape-casting

1. Introduction

Many advantages of solid oxide fuel cells (SOFCs), such as high efficiency, fuel flexibility, no use of Pt catalyst, no leakage of electrolyte, and no need for water management allow these devices to be considered as the most promising fuel cell type for next generation energy conversion systems.[1-5] The high operating temperature range (800 - 1000°C), however, causes fast thermal degradation, slow start up, and increase of the system size and component material costs.[6-8] From this viewpoint, a variety of intensive efforts to reduce the operating temperature have been made by many researchers in the past decade.

Adoption of thin film electrolytes on porous anode supports is the most common strategy to lower the operating temperature.[4,5,9-13] Thin electrolytes reduce the ohmic resistance in ion transport, resulting in an enhancement of the performance of SOFCs at lower temperatures.[12,13] Although another type of SOFCs, free-standing membrane micro-SOFCs, show highly enhanced performance at low temperatures with much reduced electrolyte thicknesses (60 - 200 nm), their weak physical strength and limited effective area hinder practical use.[14-16] In the anode support type SOFCs, the thick anode supports (typically about 1 - 2 mm) provide enough physical strength to the whole cell and enable the formation of a large effective area. In addition, the large volume of the composite anode structure provides sufficient anodic reaction sites in the cell operation.[17]

Another possible way to lower the operating temperature is to use materials with superior properties at low temperatures. Protonic ceramics, also called proton conducting oxides, are good candidates as electrolyte materials due to their high conductivity and low activation energy in the low temperature regime of ~ 600°C.[18-20] The proton mobility in the lattice oxide is preferably generated by dissociating water vapor into a hydroxide ion and a proton rather than by incorporating hydrogen into gas phase because of the energetic preference.[21-23] Hence, wet hydrogen or hydrogen containing fuels are generally used in the cell operation. Among the protonic ceramics, yttrium doped barium zirconate (BZY) has been acknowledged as the proper ceramic for the anode composite due to its excellent chemical stability under a high portion of water atmosphere.[24,25] However, it is challenging to obtain an anode support body with proper structural integrity based on BZY because the material requires a high sintering temperature.

Especially for the successful fabrication of protonic ceramic fuel cells (PCFCs) with thin electrolytes, fabrication of anode supports is very important because the anode surface crucially affects the quality of the thin electrolytes that are deposited. High roughness or microstructural artifacts like large open pores on the anode surface can cause pinholes and cracks in thin electrolytes, resulting in severe open circuit voltage (OCV) drop and cell failure.[26] Therefore, sensitive conditioning is needed before/after the anode fabrication. Thus, in the current study, a fabrication process optimization for NiO-BZY composite anode supports for

†Corresponding author : Ji-Won Son
E-mail : jwson@kist.re.kr
Tel : +82-2-958-5530 Fax : +82-2-958-5529
‡Corresponding author : Joon Hyung Shim
E-mail : shimm@korea.ac.kr
Tel : +82-2-3290-3353 Fax : +82-2-926-9290

thin-film electrolytes is performed. Thermal behaviors of the tape-casted NiO-BZY are investigated to determine optimal sintering conditions; crystallinity and microstructure are observed.

2. Experimental Procedure

Two type of anode tapes were prepared following the fabrication procedure shown in Fig. 1. One tape contained polymethyl methacrylate (PMMA) pore-formers to generate macro pores after sintering; the other did not. The latter was laminated to form an anode functional layer (AFL) on the anode body formed by the former. Commercialized powders, NiO (Sumitomo) and $BaZr_{0.85}Y_{0.15}O_{3-\delta}$ (BZY, Kceracell), were used as raw materials and mixed at a volumetric ratio of Ni:BZY = 40:60 after the reduction of NiO. Mono-dispersed PMMA (Sunjin Chemical Co.) with particle size of 5 μm was added as the pore-former to one set of the NiO-BZY powder at 30 vol%. Hypermer KD-1 (a polyester/polyamine condensation polymer, Uniqema) was added to both mixed powders as a dispersant; mixture was ball-milled for 24 h in composite solvents of ethanol and toluene with zirconia balls. Dibutyl phythalate (DBP, JUNSEI) and polyvinyl butyral B-79 (PVB-79, Monsanto) were added as a plasticizer and a binder, respectively; mixture was ball-milled again for 24 h. Tape-casting of the slurries was conducted using a customized system (STC-28C, Hansung Systems, Inc.). The thicknesses of the anode body and AFL tapes were set at 200 and 40 μm, respectively, after drying at room temperature.

One layer of the AFL tape on top of the 6 layers of the anode body tapes was laminated with a size of 5 cm × 5 cm; this was followed by uniaxial pressing under 15 MPa at 75°C for 15 min. The green tape after lamination had a thickness of 1.2 mm and was sintered at 1450°C for 10 h in ambient air. Flat NiO-BZY plates previously fabricated by powder packing and sintering at 1500°C were lain on the top and bottom of the anode tape during the sintering process.

Thermal behavior of the green tape in terms of weight loss and shrinkage profile was investigated using differential scanning calorimetry-thermal gravimetric analysis (DSC-TGA, TA Instruments DSC 2010) and dilatometric measurement (NETZSCH DIL 402C). The crystallinity of the raw powders and the sintered anode substrates was confirmed by X-ray diffraction (XRD, Bruker D8 Advance). Scanning electron microscopy (SEM, FEI SL-30 FEG) images of the surface and cross-section of the sintered anode substrate were used to observe its microstructure.

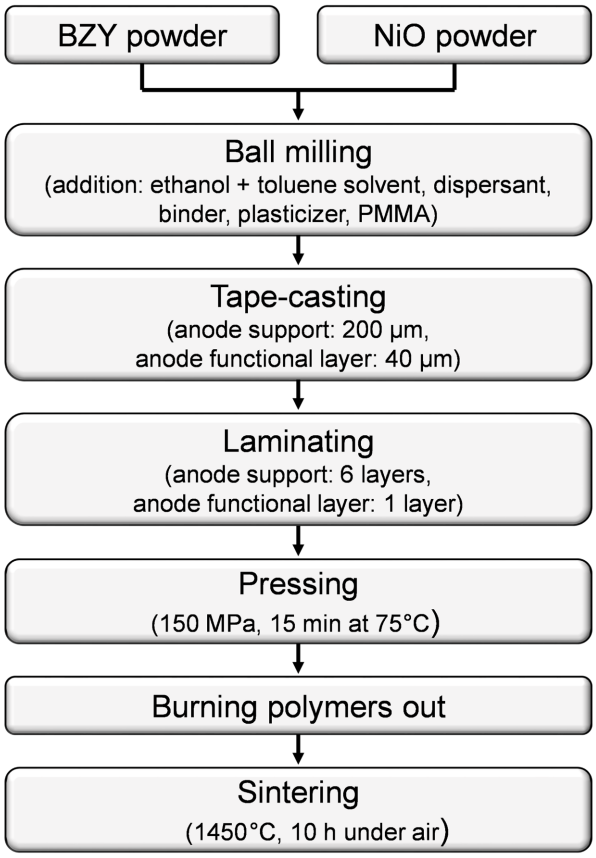

Fig. 1. Flow chart of fabrication process of the NiO-$BaZr_{0.85}Y_{0.15}O_{3-\delta}$ anode substrate via tape casting.

3. Results and Discussion

While the organic additives play important roles in the fabrication of highly dispersed and fully connected composite anode structures, these additives may introduce microstructural failures such as cracks or pin-holes during sintering.[27] Hence, sensitive conditioning in the sintering step is required to provide enough time for the additive polymers to burn out and for the constituent materials to rearrange themselves at the appropriate temperatures. To determine the burn-out schedule of the organic additives and pore-formers, DSC-TGA profiles of the green anode tape after the lamination were investigated, with results shown in Fig. 2. Two decomposition ranges was identified at

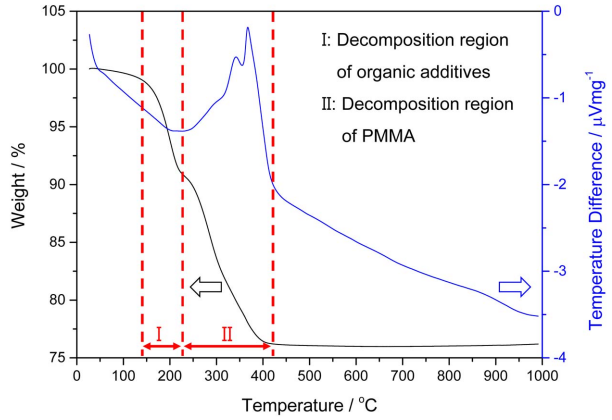

Fig. 2. Results of the differential scanning calorimetry and thermal gravimetric analyses of the NiO-$BaZr_{0.85}Y_{0.15}O_{3-\delta}$ green tape, represented by blue and black lines, respectively.

140 - 230°C and 230 - 400°C; these ranges are perfectly matched with the decomposition temperatures of the organic additives and PMMA, respectively, which can be found in the literature[28,29] and in data sheets provided by manufacturers. Thus, holding stages at the higher temperatures of 300°C and 450°C for 150 min each to sufficiently burn out the additives were put into the heating schedule; another holding stage at 600°C for 2 h was incorporated to complete the decomposition of the residual polymers.

The sintering temperature was determined by the thermal shrinkage behavior profile, which can be seen in Fig. 3. The slight expansion behavior under 1000°C might have come from sensing or calibrating errors that are frequently found in dilatometric measurement, but there was no influence on the interpretation of the sintering trend. The shrinkage of the NiO-BZY tape, which is generated by the sintering with reduction of the inter-particle distance, begins from 1000°C and has a steep slope over 1450°C. This indicates that rapid densification of the composite develops at temperatures over 1450°C. It is well-known that a high sintering temperature close to 1700°C is required to obtain fully sintered BZY, due to this material's poor sinterability.[30,31] Thus, the beginning of the shrinkage under 1300°C is mostly led by the sintering of NiO particles. According to the constraining network model of composite powders,[32] pre-sintered NiO forms a constrained matrix surrounding BZY particles and imposes compressive stresses on the BZY particles, allowing the BZY particles to be sintered at temperature lower than 1700°C. With this understanding, it can be explained that the changed shrinkage slope over 1450°C represents the simultaneous sintering of both materials. Therefore, the sintering temperature of 1450°C in the study is sufficient for the fabrication of a fully sintered NiO-BZY tape anode; the duration time was set at 10 h.

Figure 4 provides XRD patterns of the NiO (red line) and BZY (blue line) raw powders and of the NiO-BZY anode (black line) after sintering. The single phase XRD patterns of the raw powders offer good references for each component of the tape-cast anode, showing perfectly matched peak positions. This indicates that no secondary phase is generated from the NiO-BZY composite during the sintering step.

Cross-sectional SEM images of the NiO-BZY anode after sintering are provided in Fig. 5. Both layers of the AFL and anode body are clearly discernable in the low magnification SEM image given in Fig. 5(a). The thickness of the AFL was identified as being about 30 μm in the observation. It is shown that the spherical pores generated by the PMMA pore-formers are well-dispersed in the anode body and the denser AFL layer fully covers the anode body. In the high magnification SEM image provided in Fig. 5(b), the well-developed interconnectivity of the grains implies that the tape-cast anode was fully sintered under the present sintering condition. From the SEM images, good adhesion at the interface, without any cracks or delamination, between both layers (AFL and anode body) is confirmed, indicating that the fabrication conditions, including the use of organic additives, lamination, pressing, and a multistage heating schedule, are appropriate to obtain NiO-BZY anode substrate as intended.

The surface morphology of the sintered NiO-BZY AFL is presented in Fig. 6(a). Large NiO particles with a size of approximately 5 μm can be observed on the fully dense sur-

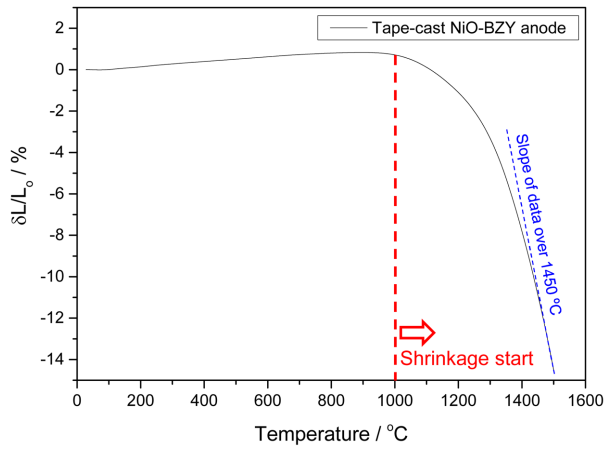

Fig. 3. Thermal shrinkage behavior of the NiO-$BaZr_{0.85}Y_{0.15}O_{3-\delta}$ green tape after lamination, obtained via dilatometric measurement.

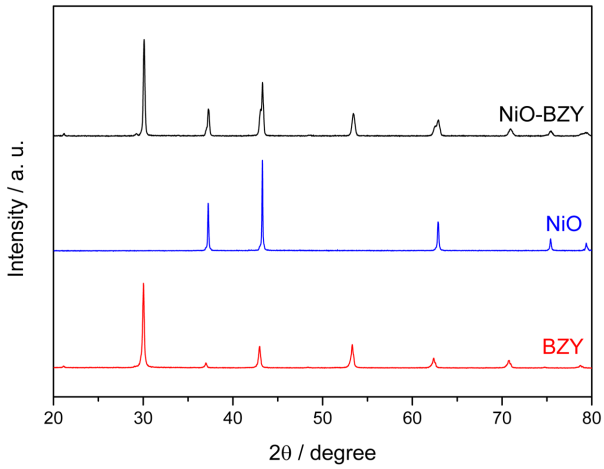

Fig. 4. X-ray diffraction patterns of the NiO and $BaZr_{0.85}Y_{0.15}O_{3-\delta}$ raw powders and of the tape-cast NiO-$BaZr_{0.85}Y_{0.15}O_{3-\delta}$ anode after sintering at 1450°C for 10 h.

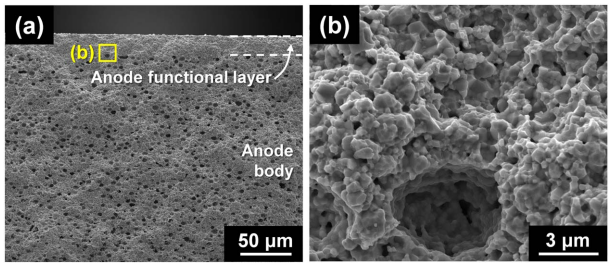

Fig. 5. Cross-sectional scanning electron microscopy images of the tape-cast NiO-$BaZr_{0.85}Y_{0.15}O_{3-\delta}$ anode after sintering at 1450°C for 10 h with (a) low and (b) high magnification.

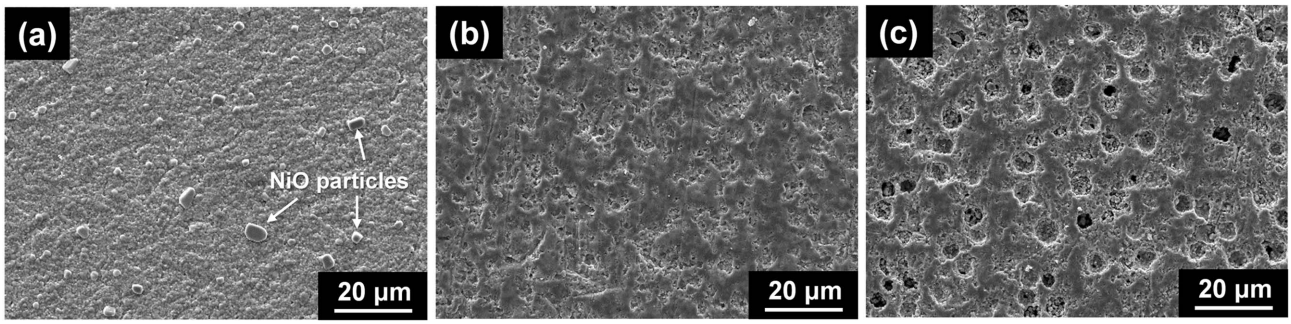

Fig. 6. Surface scanning electron microscopy images of the (a) as-sintered anode functional layer, (b) grinded anode functional layer, and (c) grinded anode body of the tape-cast NiO-$BaZr_{0.85}Y_{0.15}O_{3-\delta}$ anode after sintering at 1450°C for 10 h.

face, as shown in the SEM image. It is postulated that these larger NiO particles originate because the relatively high sintering temperature of 1450°C, due to the poor sinterability of BZY, induces excessive grain growth of the NiO phase. The over-grown NiO particles on the surface can cause discontinuity and weak interface adhesion in the deposited electrolyte film on the anode substrate. Therefore, slight surface grinding was conducted to remove the NiO particles; the surface SEM images of the AFL are provided in Fig. 6(b). A surface morphology smooth enough to accept a deposit of a dense oxide film is obtained on the AFL after grinding. If the AFL is completely polished out, the anode body is exposed and the surface morphology appears as shown in Fig. 6(c). Large pores produced by PMMA on the surface can critically harm the integrity of the thin electrolyte. Thus, it is important not to expose the anode body layer during the AFL surface grinding.

On this optimized NiO-BZY anode substrate, stable and reproducible high OCVs of around 1 V at 600°C were confirmed with merely ~ 2.5 micron-thick thin-film electrolytes, along with highly enhanced fuel cell performance;[33] on the other hand, poor OCVs below 0.4 V were observed in the thin-film PCFC fabricated on the anode substrate before optimization. These results indicate that rather careful optimization of the NiO-BZY anode is essential to achieve high performance of the PCFC, particularly when using thin electrolytes, because of the tricky sintering characteristics of BZY.

4. Conclusions

Proton conductive NiO-BZY composite anode substrate for thin film electrolytes consisting of a dense AFL and porous anode body is fabricated by the tape casting and sintering process. The multi-stage sintering conditions are optimized in the study based on measurement results from DSC-TGA and dilatometry of laminated NiO-BZY tape, resulting in an anode substrate with structural integrity. No secondary phase is found in the XRD analysis, indicating that the composite anode is obtained without any serious chemical reaction between NiO and BZY during the sintering process. In the SEM observations, it was found that the dense AFL fully covers the macro pores exposed on the surface of the anode body and induced by the PMMA pore-formers. Excessively grown NiO particles, however, are observed on the AFL surface; these are inevitably formed by the high sintering temperature of 1450°C, and thus additional grinding of the surface is required for subsequent thin film electrolyte deposition.

Acknowledgments

This work was supported by the Korea-Sweden research cooperation program (NRF-2014K1A3A1A47067412), the BK21 plus program (21A20131712520), and the Global Frontier R&D Program in the Center for Multiscale Energy Systems (NRF-2011-0031579) of the National Research Foundation (NRF) of Korea, funded by the Ministry of Science, ICT & Future Planning (MSIP). The authors are also grateful for the financial support from the Young Fellow Program of the Korea Institute of Science and Technology (KIST).

REFERENCES

1. B. C. H. Steele and A. Heinzel, "Materials for Fuel-cell Technologies," *Nature*, **414** [6861] 345-52 (2001).
2. E. D. Wachsman and K. T. Lee, "Lowering the Temperature of Solid Oxide Fuel Cells," *Science*, **334** [6058] 935-39 (2011).
3. S. C. Singhal, "Solid Oxide Fuel Cells : Designs, Materials, and Applications," *J. Korean Ceram. Soc.*, **42** [12] 777-86 (2005).
4. R. J. Gorte, S. Park, J. M. Vohs, and C. Wang, "Anodes for Direct Oxidation of Dry Hydrocarbons in a Solid-oxide Fuel Cell," *Adv. Mater.*, **12** [19] 1465-69 (2000).
5. Z. Shao, S. M. Haile, J. Ahn, P. D. Ronney, Z. Zhan, and S. A. Barnett, "A Thermally Self-sustained Micro Solid-oxide Fuel-cell Stack with High Power Density," *Nature*, **435** [7043] 795-98 (2005).
6. H. Yokokawa, T. Horita, K. Yamaji, H. Kishimoto, and M. E. Brito, "Degradation of SOFC Cell/Stack Performance in Relation to Materials Deterioration," *J. Korean Ceram. Soc.*, **49** [1] 11-8 (2012).
7. K. Park, S. Yu, J. Bae, H. Kim, and Y. Ko, "Fast Perfor-

mance Degradation of SOFC Caused by Cathode Delamination in Long-term Testing," *Int. J. Hydrogen Energ.*, **35** [16] 8670-77 (2010).
8. Y.-S. Chou and J. W. Stevenson, "Thermal Cycling and Degradation Mechanisms of Compressive Mica-based Seals for Solid Oxide Fuel Cells," *J. Power Sources*, **112** [2] 376-83 (2002).
9. H.-S. Noh, J.-W. Son, H. Lee, H.-R. Kim, J.-H. Lee, and H.-W. Lee, "Thin Film $(La_{0.7}Sr_{0.3})_{0.95}MnO_{3-\delta}$ Fabricated by Pulsed Laser Deposition and Its Application as a Solid Oxide Fuel Cell Cathode for Low-temperature Operation," *J. Korean Ceram. Soc.*, **47** [1] 75-81 (2010).
10. H.-S. Noh, J.-W. Son, H. Lee, H.-S. Song, H.-W. Lee, and J.-H. Lee, "Low Temperature Performance Improvement of SOFC with Thin Film Electrolyte and Electrodes Fabricated by Pulsed Laser Deposition," *J. Electrochem. Soc.*, **156** [12] B1484-90 (2009).
11. H.-S. Noh, J.-W. Son, H. Lee, H.-I. Ji, J.-H. Lee, and H.-W. Lee, "Suppression of Ni Agglomeration in PLD Fabricated Ni-YSZ Composite for Surface Modification of SOFC Anode," *J. Eur. Ceram. Soc.*, **30** [16] 3415-23 (2010).
12. Y. J. Leng, S. H. Chan, K. A. Khor, and S. P. Jiang, "Performance Evaluation of Anode-supported Solid Oxide Fuel Cells with Thin Film YSZ Electrolyte," *Int. J. Hydrogen Energ.*, **29** [10] 1025-33 (2004).
13. A. Leonide, V. Sonn, A. Weber, and E. Ivers-Tiffée, "Evaluation and Modeling of the Cell Resistance in Anode-Supported Solid Oxide Fuel Cells," *J. Electrochem. Soc.*, **155** [1] B36-41 (2008).
14. J. H. Shim, C. C. Chao, H. Huang, and F. B. Prinz, "Atomic Layer Deposition of Yttria-stabilized Zirconia for Solid Oxide Fuel Cells," *Chem. Mater.*, **19** [15] 3850-54 (2007).
15. A. Evans, A. Bieberle-Hütter, J. L. M. Rupp, and L. J. Gauckler, "Review on Microfabricated Micro-solid Oxide Fuel Cell Membranes," *J. Power Sources*, **194** [1] 119-29 (2009).
16. K. Bae, D. Y. Jang, H. J. Jung, J. W. Kim, J. W. Son, and J. H. Shim, "Micro Ceramic Fuel Cells with Multilayered Yttrium-doped Barium Cerate and Zirconate Thin Film Electrolytes," *J. Power Sources*, **248** 1163-69 (2014).
17. S. Primdahl and M. Mogensen, "Oxidation of Hydrogen on Ni/Yttria-Stabilized Zirconia Cermet Anodes," *J. Electrochem. Soc.*, **144** [10] 3409-19 (1997).
18. H. Iwahara, "Proton Conducting Ceramics and Their Applications," *Solid State Ionics*, **86-8** 9-15 (1996).
19. H. G. Bohn and T. Schober, "Electrical Conductivity of the High-temperature Proton Conductor BaZr(0.9)Y(0.1)O(2.95)," *J. Am. Ceram. Soc.*, **83** [4] 768-72 (2000).
20. K. D. Kreuer, "Proton-conducting Oxides," *Annu. Rev. Mater. Res.*, **33** 333-59 (2003).
21. S.-J. Song, E. D. Wachsman, S. E. Dorris, and U. Balachandran, "Defect Chemistry Modeling of High-temperature Proton-conducting Cerates," *Solid State Ionics*, **149** [1-2] 1-10 (2002).
22. T. Schober, W. Schilling, and H. Wenzl, "Defect Model of Proton Insertion into Oxides," *Solid State Ionics*, **86-88 Part 1** 653-58 (1996).
23. H. I. Ji, B. K. Kim, J. H. Yu, S. M. Choi, H. R. Kim, J. W. Son, H. W. Lee, and J. H. Lee, "Three Dimensional Representations of Partial Ionic and Electronic Conductivity Based on Defect Structure Analysis of BaZr0.85Y0.15O3-delta," *Solid State Ionics*, **203** [1] 9-17 (2011).
24. K. H. Ryu and S. M. Haile, "Chemical Stability and Proton Conductivity of Doped $BaCeO_3$–$BaZrO_3$ Solid Solutions," *Solid State Ionics*, **125** [1-4] 355-67 (1999).
25. S. Barison, M. Battagliarin, T. Cavallin, L. Doubova, M. Fabrizio, C. Mortalo, S. Boldrini, L. Malavasi, and R. Gerbasi, "High Conductivity and Chemical Stability of $BaCe_{1-x-y}Zr_xY_yO_{3-\delta}$ Proton Conductors Prepared by a Sol-gel Method," *J. Mater. Chem.*, **18** [42] 5120-28 (2008).
26. C. W. Kwon, J. W. Son, J. H. Lee, H. M. Kim, H. W. Lee, and K. B. Kim, "High-performance Micro-solid Oxide Fuel Cells Fabricated on Nanoporous Anodic Aluminum Oxide Templates," *Adv. Funct. Mater.*, **21** [6] 1154-59 (2011).
27. A. Mukherjee, B. Maiti, A. Das Sharma, R. N. Basu, and H. S. Maiti, "Correlation between Slurry Rheology, Green Density and Sintered Density of Tape Cast Yttria Stabilised Zirconia," *Ceram. Int.*, **27** [7] 731-39 (2001).
28. H. Moon, S. D. Kim, S. H. Hyun, and H. S. Kim, "Development of IT-SOFC Unit Cells with Anode-supported Thin Electrolytes via Tape Casting and Co-firing," *Int. J. Hydrogen Energ.*, **33** [6] 1758-68 (2008).
29. X. Huang and W. J. Brittain, "Synthesis and Characterization of PMMA Nanocomposites by Suspension and Emulsion Polymerization," *Macromolecules*, **34** [10] 3255-60 (2001).
30. P. Babilo, T. Uda, and S. M. Haile, "Processing of Yttrium-doped Barium Zirconate for High Proton Conductivity," *J. Mater. Res.*, **22** [5] 1322-30 (2007).
31. P. Babilo and S. M. Haile, "Enhanced Sintering of Yttrium-doped Barium Zirconate by Addition of ZnO," *J. Am. Ceram. Soc.*, **88** [9] 2362-68 (2005).
32. F. F. Lange, "Constrained Network Model for Predicting Densification Behavior of Composite Powders," *J. Mater. Res.*, **2** [01] 59-65 (1987).
33. K. Bae, D. Y. Jang, H.-S. Noh, H. J. Kim, J. Hong, K. J. Yoon, B.-K. Kim, J.-W. Son, and J. H. Shim, "High-performance Protonic Ceramic Fuel Cells with Thin-film Yttriumdoped Barium Zirconate Electrolyte and Nickel Oxide–Yttrium-doped Barium Zirconate Interlayers," *Adv. Energy Mater.*, submitted.